

# *In-situ* generation and analysis of charge transfer materials using an OTTLE cell and resonance Raman scattering†

Rachael E. Littleford,<sup>a</sup> Michael A. J. Paterson,<sup>b</sup> Paul J. Low,<sup>b</sup> Daniel R. Tackley,<sup>c</sup> Linda Jayes,<sup>c</sup> Geoffrey Dent,<sup>c</sup> Julian C. Cherryman,<sup>c</sup> Bev Brown<sup>c</sup> and W. Ewen Smith<sup>\*a</sup>

<sup>a</sup> University of Strathclyde, Department of Pure and Applied Chemistry, 295 Cathedral Street, Glasgow, UK G1 1XL

<sup>b</sup> Department of Chemistry, University of Durham, South Road, Durham, UK DH1 3LE

<sup>c</sup> Avecia Ltd., Hexagon House, Blackley, Manchester, UK M9 8ZS

Received 10th February 2004, Accepted 23rd March 2004

First published as an Advance Article on the web 25th May 2004

Poly(aryl)amine based charge transfer materials (CTMs) are essential components in a range of present and future technologies, from the Xerox process to display devices based upon light emitting polymers (LEPs). However, there is a lack of detailed understanding regarding the electronic properties of CTMs in their various neutral and oxidized forms. This paper reports the use of an optically transparent thin layer electrochemical (OTTLE) cell in combination with a Raman microprobe system and DFT calculations to provide information on the molecular and electronic structure of the mono- and di-oxidized derivatives of the classic CTM *N,N'*-diphenyl-*N,N'*-bis(3-methylphenyl)(1,1'-biphenyl)-4,4'-diamine (TPD) and the closely related species *N,N'*-diphenyl-*N,N'*-bis(2,4-dimethylphenyl)(1,1'-biphenyl)-4,4'-diamine (DMTPD). The resonance Raman scattering profile easily discriminates between the monovalent and divalent cations while DFT calculations permit correlation of the observed vibrational frequencies with localized atomic displacements. The cations are best described in terms of a symmetrical (*i.e.* fully delocalized) structure. The high sensitivity of the method suggests that it should be appropriate for the observation of low concentrations of the various cations generated from TPD type CTMs during device operation.

## Introduction

Poly(aryl)amine based charge transfer materials (CTMs) are used in established technologies, such as the Xerox process, and also have immense potential for application in the construction of light emitting polymer (LEP) based display devices.<sup>1–7</sup> However, the design of these compounds for both present and future application would be significantly aided by a detailed understanding of the electronic and physical properties of these materials, not only in their neutral state, but also in the ‘active’ oxidised forms which play a role in the charge transfer process.<sup>8–10</sup>

Since charge transport through a molecular (or polymeric) material depends upon interactions between the molecular (or polymeric) units, compounds that form strictly amorphous phases have been the source of the most intense investigation. An unfortunate consequence of this is that there is little structural information in the open literature relating to the molecular structure of even simple poly(aryl)amines,<sup>11,12</sup> and structural data relating to the oxidized forms of these materials is extremely rare. In the absence of crystalline samples for structural analysis, the majority of current research has utilized computational methods to explore the geometry and electronic structure of model CTMs and their oxidized derivatives.<sup>13–17</sup>

In addition to the intermolecular electron transfer events between neutral molecules and their radical cation counterparts, which are related to charge mobility in the bulk sample, intramolecular electron transfer events within tetra(aryl)benzidine “mixed valence” radical cations have been a source of

interest of late. These systems often contain a characteristic transition in the near-infrared region,<sup>18</sup> which in the simplest terms, can be related to the photoinduced intramolecular electron transfer between the amine centres.<sup>12</sup> However, since the orbitals involved in this transition can be delocalized and involve considerable aryl and nitrogen character, the interpretation of this data can be challenging.<sup>18–22</sup>

Raman spectroscopy offers an effective method through which to interrogate the structure of poly(aryl)amine based CTMs such as *N,N'*-diphenyl-*N,N'*-bis(3-methylphenyl)(1,1'-biphenyl)-4,4'-diamine (TPD, **1**) and the closely related species *N,N'*-diphenyl-*N,N'*-bis(2,4-dimethylphenyl)(1,1'-biphenyl)-4,4'-diamine (DMTPD, **2**).<sup>23–27</sup> The neutral forms of these molecules are readily accessible, while spectroelectrochemical techniques provide a solution to the problem of obtaining the radical samples for study,<sup>28–35</sup> and by using an optically transparent thin layer electrochemical (OTTLE) cell a solution of the radical cations may be generated in the spectrometer beampath and analyzed *in-situ*. In the particular case of the Raman experiments described here, excitation frequencies were chosen after consideration of the absorption spectra of the monovalent and divalent cations of species **1** and **2** (**1**<sup>•+</sup> and **2**<sup>•+</sup>), which have also been obtained by spectroelectrochemical methods.<sup>12</sup> In combination with DFT calculations, which can be used to correlate the Raman vibrational frequencies with the atomic displacements associated with each vibration, the method provides information on the structure and electronic structure of the oxidized forms of these CTMs *in-situ*.

## Experimental

TPD and DMTPD were prepared by minor variation of literature methods.<sup>36</sup>

† Electronic supplementary information (ESI) available: BPW91/6-31G(d) predicted vibrational frequencies and intensities for the neutral, radical cation and dication species of **1** and **2**. See <http://www.rsc.org/suppdata/cp/b4/b402015d/>

Spectroelectrochemical studies were carried out in an OTTLE cell (quartz, 1 mm pathlength) of standard design fitted with a platinum gauze working electrode and platinum wire counter and pseudo-reference electrodes<sup>37</sup> using a 0.5 mM solution of the material of interest with supporting electrolyte of tetrabutylammonium tetrafluoroborate (0.1 M) in freshly distilled dichloromethane at room temperature. Potentials were obtained from conventional cyclic voltammetry experiments, using the same solvent and a similar all-platinum electrode set, and are quoted against SCE using a ferrocene internal standard such that the ferrocene–ferrocenium couple falls at 0.46 V.<sup>38</sup>

Electronic spectra were recorded on a Varian Cary 5 spectrophotometer.

Raman spectra were collected using Renishaw 2000 micro-probe systems with a Spectra-Physics model 163 argon-ion laser providing excitation at 514.5 nm, and a Spectra-Physics model 127 helium–neon laser providing excitation at 632.7 nm. The OTTLE cell was mounted in the beampath of the spectrometer and the laser focused onto a pore within the gauze working electrode using the microscope. *In-situ* spectra were collected using 1 accumulation of 1 s. Raman spectra of the solid CTM were the result of three 10-s accumulations. Data collection and manipulation used GRAMS software.

Calculations were performed using the Gaussian 98W software package.<sup>39</sup> For each molecule the geometry was optimised and frequency-intensity (including Raman) calculations were run for the neutral, radical cation (charge = 1, multiplicity = 2) and dication (charge = 2, multiplicity = 1) states at a DFT level using the BPW91 method (Becke's 1988 exchange functional<sup>40</sup> with Perdew and Wang's 1991 gradient-corrected correlation functional).<sup>41</sup> The 6-31G(d) basis set was used for all calculations.<sup>42–46</sup> Vibrational spectra were simulated from the frequency-intensity point data by adding a mixed (1:1) Gaussian : Lorentzian lineshape with a fixed linewidth of 6 cm<sup>-1</sup>.

## Results

### Electrochemical response

We have previously described the electrochemical response of **1** and **2**, and observed two, one electron waves associated with the stepwise formation of the mono- (**1**  $E_{1/2} = 0.292$  V, **2**  $E_{1/2} = 0.250$  V) and di-cations (**1**  $E_{1/2} = 0.507$  V, **2**  $E_{1/2} = 0.505$  V).<sup>12</sup> The large potential difference between the two redox processes for **1** (215 mV) and **2** (255 mV) give rise to significantly large comproportionation constants,  $K_C$  and indicate the high thermodynamic stability of the radical cations **1**<sup>+</sup> ( $K_C = 4300$ ) and **2**<sup>+</sup> ( $K_C = 20\,500$ ).

### Resonance Raman scattering

The electronic spectra of the cations are shown in Fig. 1.<sup>12</sup> Both the monovalent and divalent cations are coloured and consequently resonance Raman scattering should provide a good *in-situ* probe for the appearance of the ions, providing both vibrational and electronic information.

For **1**<sup>+</sup>, excitation at 514.5 nm falls within the absorption band envelope centred at 477 nm. As the excitation wavelength lies towards the lower energy side of the absorption band this will be close to the 0 → 0 and 0 → 1 vibronic band frequencies, and consequently should be effective in creating resonance enhancement. In the case of **1**<sup>2+</sup>, excitation at 632.7 nm falls within the absorption envelope which has its maximum at 732 nm, therefore resonance enhancement would be expected. However, since the 632.7 nm excitation wavelength is on the high-energy side of the absorption band, higher vibronic levels associated with this will be closest;

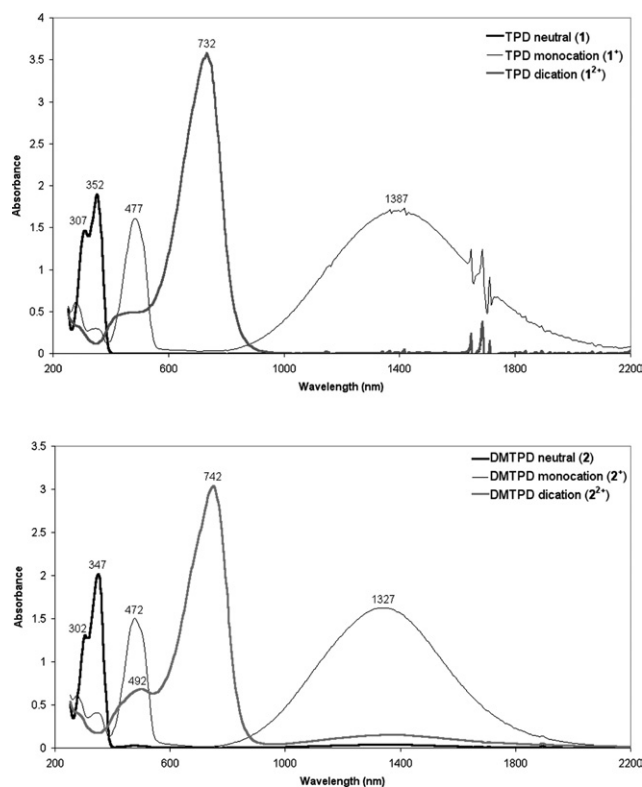


Fig. 1 Electronic spectra of the neutral species and the monovalent and divalent cations of TPD (**1**) and DMTPD (**2**). Spectra taken at voltages appropriate to the formation of each species.

consequently weaker resonance enhancement is to be expected. However, for the divalent species 514.5 nm excitation would be expected to give even less enhancement, consequently, for the divalent species 632.7 nm should still give the greatest enhancement.

The absorption profiles associated with **2**<sup>n+</sup> are similar to those of **1**<sup>n+</sup>, and while there are small shifts in the electronic absorption maxima, resonant enhancement of the Raman spectra will still be achieved with 514.5 nm (**2**<sup>+</sup>) or 632.7 nm (**2**<sup>2+</sup>) excitation.

The Raman spectra of a solid sample of **2** and **2**<sup>+</sup>, prepared chemically,<sup>12,36</sup> were collected using a 514.5 nm excitation wavelength (Fig. 2(a) and (b)) in order to assess the relevance of the solution based OTTLE spectra to the solid state. In the case of neutral **2**, the spectrum is dominated by the large bands at 1614 and 1606 cm<sup>-1</sup>, and other strong bands at 1294 and 1182 cm<sup>-1</sup>. The distinctly different spectrum of **2**<sup>+</sup> in the solid state clearly indicates the ability of Raman scattering as a “fingerprint” technique in discriminating the CTM in these oxidation states. Spectra (b) and (c) show that there is a strong similarity between the solid state and OTTLE cell spectra, giving confidence that the solution state spectra can be accurately assigned.

The OTTLE cell enabled the observation of the monovalent and divalent cations of **1** and **2** *in-situ*. In the case of **2**<sup>+</sup>, which is illustrated in Fig. 2(c), the solution state spectra compare well with those obtained from the solid samples. The Raman spectra of the electrochemically generated series **2**<sup>n+</sup> recorded using excitation at 514.5 nm (Fig. 3(a)) and 632.7 nm (Fig. 3(b)) show the general trends, with the solvent band at ~695 cm<sup>-1</sup> providing a useful internal reference for the relative intensity of the sample bands. As well as obvious increases in intensity in the Raman scattering due to resonance enhancement as the mono- ( $\lambda_{\text{ex}} = 514.5$  nm) and di-cations ( $\lambda_{\text{ex}} = 632.7$  nm) are formed, there is clear evidence of overtones in the region between 1600 and 3200 cm<sup>-1</sup> in Fig. 3(a). The presence of overtones is common for resonant systems

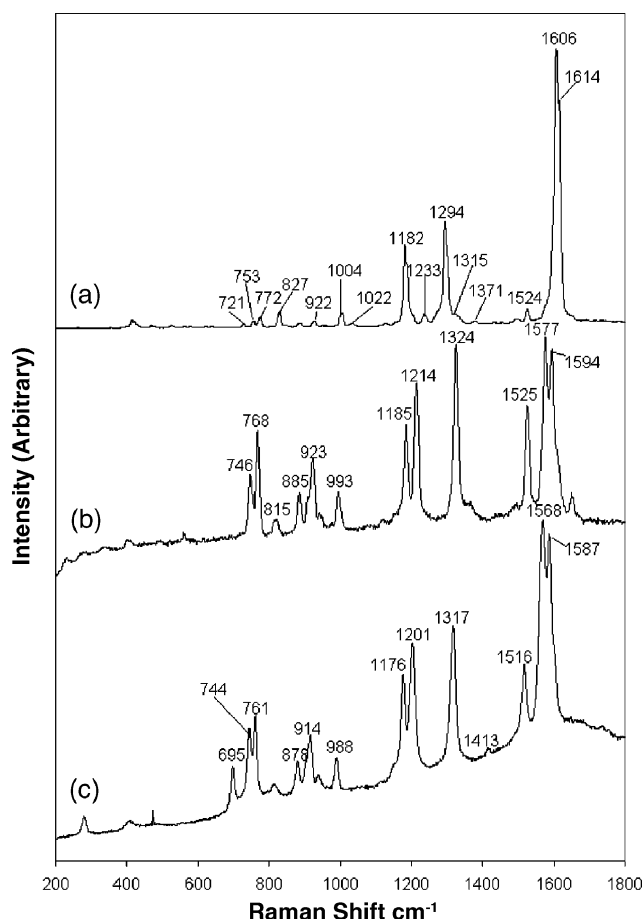


**Fig. 2** Experimental Raman spectra of DMTPD: (a) neutral solid, (b) monocation solid and (c) monocation in solution. Excitation at 514.5 nm.

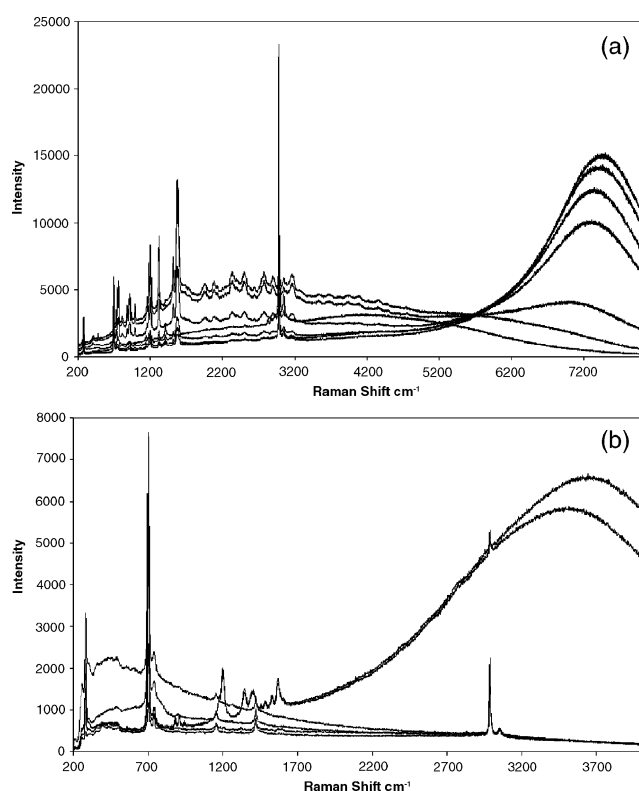


**Fig. 3** Raman spectra showing the generation of the DMTPD monocation and dication *in-situ* inside an OTTLE cell. Excitation at (a) 514.5 nm and (b) 632.7 nm.

since the selection rule preventing overtones is not applicable for A term scattering, and is less rigorous for B term.<sup>47</sup>

A broad emission profile around  $7400\text{ cm}^{-1}$  (514.5 nm excitation), or  $3700\text{ cm}^{-1}$  (632.7 nm excitation) accompanies the Raman bands associated with  $2^{2+}$ . This appears to be a standard emission process with a maximum at about 826 nm, based on absorption and emission from the transition which gives rise to the absorption band at 742 nm (Fig. 1). In the case of 514.5 nm excitation, there also appears to be emission from the monocation with a maximum at approximately  $2500\text{ cm}^{-1}$  lower than the excitation wavelength which is less easily explained because of the lower energy electronic transition. However, Raman scattering uses a high-power laser for excitation, and emission from higher excited states is known. This will be helped by the large energy separation between the monocation absorption band at 472 nm and the near infrared absorption band at 1327 nm. This emission is broad compared to that of the dication.

The frequencies of the Raman active modes of  $2^+$  are similar, but not identical, to those of  $2^{2+}$  (Fig. 4(a) and (b)) and there are significant intensity changes in individual bands, particularly in the 1600 and 1200  $\text{cm}^{-1}$  regions. The lower intensity of the  $2^{2+}$  bands with 514.5 nm excitation wavelength may indicate the much weaker resonance enhancement at this excitation wavelength.

Figs. 5 and 6 show the results of an OTTLE experiment using **1**. An obvious increase in intensity in the Raman scattering occurs when the electrochemically generated species fall in resonance with the excitation wavelength. Thus, excitation at 632.7 nm results in very little resonance enhancement from the monocation, but greater enhancement from the dication. It is therefore clear that resonance Raman scattering offers a convenient method for the detection of the oxidized forms of poly(aryl)amine based CTMs within a complex mixture. However, in order to derive structural information relating to the various species which may be generated electrochemically and detected by resonance Raman spectroscopy it is necessary

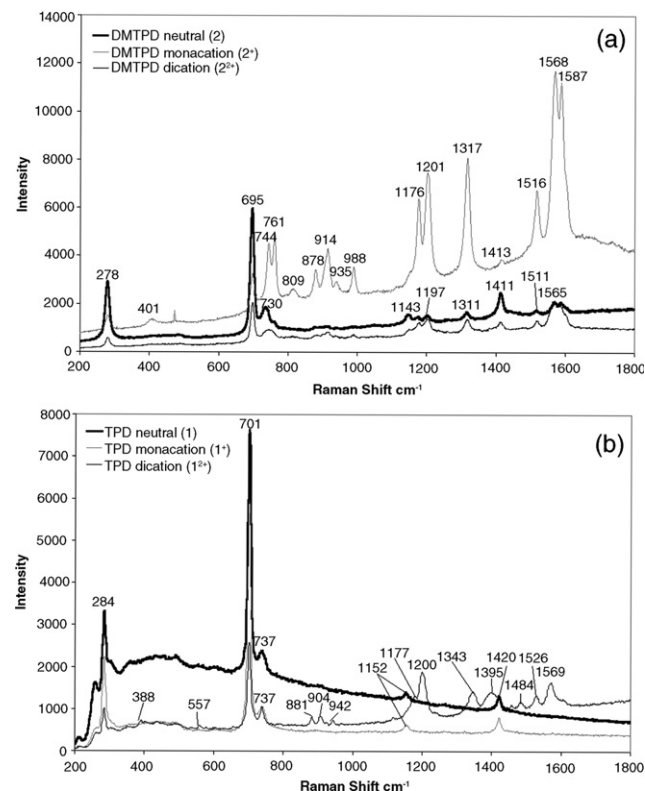


**Fig. 4** Selected Raman spectra showing the generation of the DMTPD monocation and dication *in-situ* inside an OTTLE cell. Excitation at (a) 514.5 nm and (b) 632.7 nm.

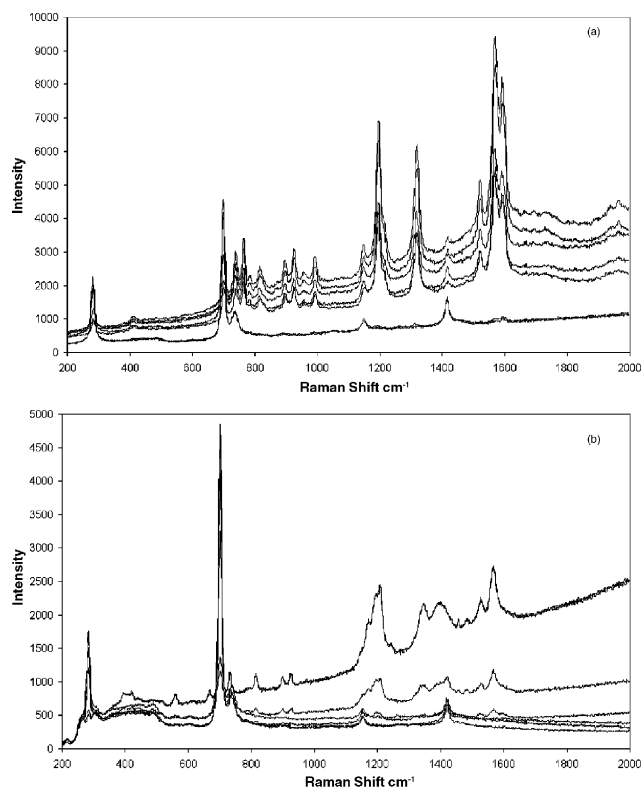


**Fig. 5** Raman spectra showing the generation of the TPD monocation and dication *in-situ* inside an OTTLE cell. Excitation at (a) 514.5 nm and (b) 632.7 nm.

to turn to DFT based methods to provide a correlation between the electronic transitions responsible for the resonance enhancement, the observed molecular (Raman) vibrational frequencies and the atomic displacements.

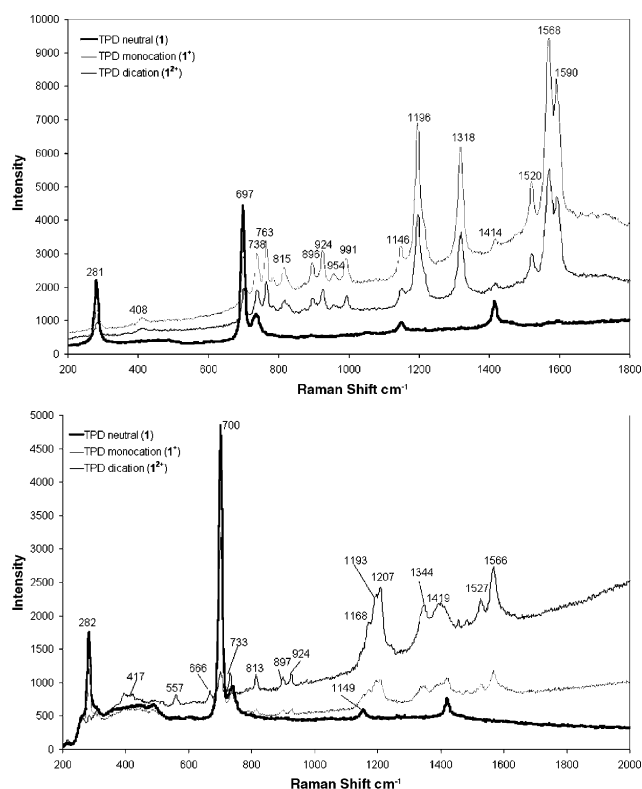


**Fig. 6** Selected Raman spectra showing the generation of the TPD monocation and dication *in-situ* inside an OTTLE cell. Excitation at 514.5 nm (top) and 632.7 nm (foot).

## DFT calculations

Given the similarities of the experimental spectra of  $1^{n+}$  and  $2^{n+}$ , the Raman active vibrations of  $2^{n+}$  were modelled using DFT methods as described in the Experimental section. Allowing for the minor errors which are inherent in the calculations arising from the neglect of solvent effects, the calculated spectral frequencies are expected to be relevant to both systems. The solid-state Raman spectra (Fig. 2(a) and (b)) were selected for comparison with the calculated neutral and  $2^+$  spectra in Fig. 7 because of the better signal to noise ratio. However, due to the instability of the  $2^{2+}$  species in the solid state, the solution phase resonance Raman spectrum obtained from generation of the dication in the OTTLE cell (Fig. 4(b)) is used. There is close agreement between the calculated and observed vibrational frequencies in the region 400 to 1800  $\text{cm}^{-1}$ . In the case of the neutral systems the largest difference between the experimental and calculated frequencies for any clearly assigned band was 21  $\text{cm}^{-1}$ , and a fit of the ten most intense bands gave an average error of 8.4  $\text{cm}^{-1}$ . A similar comparison of the theoretical result with spectra from the monocation (Fig. 2(b)) reveals the largest mismatch for any band was 37  $\text{cm}^{-1}$ , with an average error of 8.9  $\text{cm}^{-1}$  for the ten most intense bands. For the dication, the largest error for any one band is 18  $\text{cm}^{-1}$ , with an average error of 7.1  $\text{cm}^{-1}$  for all assigned bands. Thus, the frequency assignments as made by the DFT calculations can be used with some confidence. However, the intensity values calculated do not fit well with the experimental values. This is quite common with current calculations, and in this case it must also be borne in mind that the calculations are for normal Raman scattering in the gas phase and the spectra obtained from the cations are due to

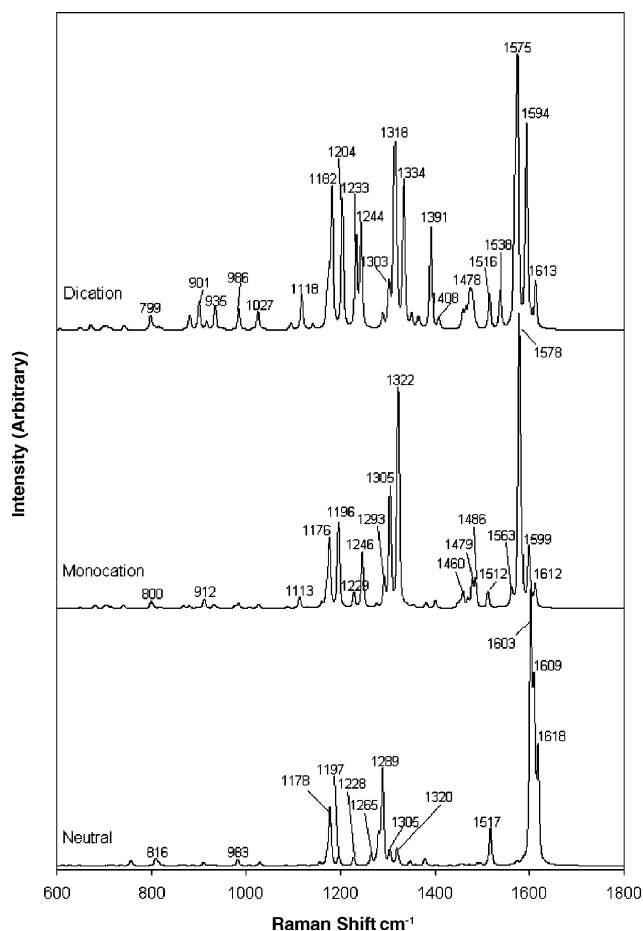


**Fig. 7** Predicted Raman spectrum of neutral, monocation and dication DMTPD.

resonance Raman scattering in the solution and solid phase. Lists of calculated band frequencies together with the experimental frequencies and the atomic displacements to which the Raman active bands may be assigned are given in Tables 1–3.<sup>48</sup> A full listing of all of the calculated vibrational

frequencies for the neutral, radical cation and dication species is available as ESI.†

## Discussion

The Raman spectra of **2** and **2**<sup>+</sup> in the solid state are given in Fig. 2. On the basis of the DFT calculations, the bands between 1550 and 1620 cm<sup>-1</sup> can be assigned to the quadrant stretches of all the phenyl ring systems. The main differences in the spectra lie in the relative intensity of the bands between

**Table 1** Assignment of neutral DMTPD<sup>48</sup>

Experimental/ cm <sup>-1</sup>	Calculated <sup>a</sup> / cm <sup>-1</sup>	Assignment
1614 (s)	1618	Quadrant str. on all rings + C–N str. + biphenyl str.
	<i>1609</i>	Quadrant str. on all rings + C–N str. + biphenyl str.
1606 (s)	1603	Quadrant str. on all rings except dimethyl + C–N str. + biphenyl str.
1524 (m)	1517	Biphenyl str.
1488 (w)	<i>1496</i>	Dimethyl rings deformation + C–N str.
	1489	Non-dimethyl rings deformation + C–N str.
1371 (w)	1380	Methyl C–H wag
	<i>1377</i>	Methyl C–H wag
1322 (sh, w)	1320	Biphenyl str + biphenyl rings breathing + C–N str. + non-dimethyl rings C–H wag
1315 (sh, w)	1304	Biphenyl rings C–H wag + C–N str.
1294 (s)	<i>1289</i>	Biphenyl str. + biphenyl rings C–H wag + non-dimethyl rings C–H wag
	1281	Biphenyl str. + biphenyl rings C–H wag + non-dimethyl rings C–H wag
	1275	Biphenyl rings C–H wag + dimethyl rings C–H wag
	1264	C–N str. + all rings C–H wag
1233 (m)	1228	Dimethyl rings deformation + C–H wag
1182 (s)	1196	C–N str. + all rings deformation
	<i>1178</i>	All rings deformation
	1173	Mainly non-dimethyl rings C–H wag
1150 (sh, w)	<i>1157</i>	Dimethyl and non-dimethyl rings C–H wag
	1156	Dimethyl and non-dimethyl rings C–H wag
1022 (w)	<i>1030</i>	Non-dimethyl rings deformation
	1028	Methyl C–H wag
1004 (m)	983	Non-dimethyl rings deformation
922 (w)	924	C–H wag on biphenyl and dimethyl rings
	<i>910</i>	Deformation on all non-dimethyl rings + dimethyl rings C–H wag
827 (m)	816	C–H wag on biphenyl and non-dimethyl rings
	<i>810</i>	C–H wag on biphenyl rings
	807	C–H wag on all rings
772 (w)	–	
753 (w)	757	Biphenyl rings deformation + dimethyl rings C–H wag
721 (w)	711	Dimethyl rings deformation
413 (w)	459	Mainly ring deformation and C–H wag on dimethyl rings
	422	Movements on all rings
	406	Deformation on biphenyl and non-dimethyl rings

s = Strong, m = medium, w = weak, sh = shoulder. <sup>a</sup> The most intense of the calculated vibrations is italicised.

**Table 2** Assignment of DMTPD<sup>•+</sup> (Radical cation)

Experimental/ cm <sup>-1</sup>	Calculated <sup>a</sup> / cm <sup>-1</sup>	Assignment
1649 (w)	1612	Quadrant str. on all rings + C–N str. + biphenyl str.
1594 (s)	1599	Quadrant str. on all rings + C–N str. + biphenyl str.
1577 (s)	<i>1583</i>	Quadrant str. on all rings except dimethyl + C–N str. + biphenyl str.
	1578	Quadrant str. on all rings except dimethyl + C–N str. + biphenyl str.
	1562	Quadrant str. on dimethyl rings
1525 (m)	1512	Biphenyl str. + biphenyl rings deformation + C–N str.
1490 (w)	<i>1485</i>	Dimethyl rings deformation + C–N str.
	1479	Non-dimethyl rings deformation + C–N str.
	1469	Methyl C–H scissoring
	1460	All rings except dimethyl deformation + methyl C–H scissoring
1366 (sh, w)	1381	Methyl C–H wag
1324 (s)	<i>1322</i>	Biphenyl str. + biphenyl rings breathing + C–N str. + non-dimethyl rings C–H wag
	1305	Biphenyl str. + biphenyl rings breathing + C–N str. + non-dimethyl rings C–H wag
	1303	Biphenyl str. + biphenyl rings breathing + C–N str. + non-dimethyl rings C–H wag
	1293	Biphenyl rings C–H wag + C–N str. + non-dimethyl rings C–H wag
–	1246	Biphenyl rings C–H wag + C–N str. + dimethyl and non-dimethyl rings breathing
–	1229	Mainly dimethyl rings breathing
1214 (m)	1196	C–N str. + all rings C–H wag
1185 (m)	<i>1176</i>	C–N str. + all rings C–H wag
	1171	Mainly non-dimethyl rings C–H wag
	1160	Mainly non-dimethyl rings C–H wag
1119 (w)	1113	Biphenyl rings C–H wag and dimethyl rings C–H wag
993 (w)	985	Non-dimethyl rings deformation
923 (m)	932	C–H wag on biphenyl and dimethyl rings
	<i>912</i>	Biphenyl rings deformation + C–H wag on dimethyl and non-dimethyl rings
815 (w)	800	C–H wag on biphenyl rings

s = Strong, m = medium, w = weak, sh = shoulder. <sup>a</sup> The most intense of the calculated vibrations is italicised.

**Table 3** Assignment of DMTPD<sup>2+</sup> (Dication, Singlet)

Experimental/ cm <sup>-1</sup>	Calculated <sup>a</sup> / cm <sup>-1</sup>	Assignment
1569 (m)	1594	Quadrant str. on all rings + C–N str. + biphenyl str.
	<i>1575</i>	Quadrant str. on all rings except dimethyl + C–N str. + biphenyl str.
	1569	Quadrant str. on all rings except dimethyl + biphenyl str.
1526 (w)	<i>1538</i>	Quadrant str. on dimethyl rings
	1516	Biphenyl str. + biphenyl rings deformation + C–N str.
	1515	Biphenyl str. + biphenyl rings deformation + C–N str.
1484 (w)	1481	Methyl C–H scissoring
	1478	Methyl C–H scissoring + non-dimethyl rings C–H wag + C–N str.
	<i>1473</i>	All rings C–H wag + dimethyl C–H scissoring
1395 (m)	1391	Methyl C–H wag
1343 (m)	<i>1334</i>	Biphenyl str. + biphenyl rings deformation + C–N str. + non-dimethyl rings C–H wag
	1318	Biphenyl str. + biphenyl rings deformation + C–N str. + non-dimethyl rings C–H wag
	1314	Biphenyl str. + biphenyl rings deformation + C–N str. + non-dimethyl rings C–H wag
	1303	Biphenyl rings C–H wag + C–N str. + non-dimethyl rings C–H wag
–	1244	Biphenyl rings C–H wag + C–N str. + dimethyl and non-dimethyl rings breathing
–	1233	Mainly dimethyl rings breathing
1200 (s)	1204	Biphenyl str. + C–N str. + all rings C–H wag
	<i>1182</i>	Biphenyl str. + C–N str. + all rings C–H wag
1177 (sh, m)	<i>1176</i>	Dimethyl and non-dimethyl rings C–H wag
	1172	All rings C–H wag
	1118	Biphenyl rings C–H wag and dimethyl rings C–H wag
942 (w)	935	Dimethyl rings deformation
904 (w)	901	Biphenyl rings deformation + C–H wag on non-dimethyl rings
881 (w)	881	C–H wag on dimethyl and non-dimethyl rings

s = Strong, m = medium, w = weak, sh = shoulder. <sup>a</sup> The most intense of the calculated vibrations is italicised.

1350 and 1200 cm<sup>-1</sup>. Both the relatively intense band at 1294 cm<sup>-1</sup> in **2** and the relatively intense band at 1324 cm<sup>-1</sup> in **2**<sup>+</sup> arise from a combination of C–N and C–C stretches. The main difference between the 1294 cm<sup>-1</sup> mode (**2**) and the 1324 cm<sup>-1</sup> mode (**2**<sup>+</sup>) is that the **2**<sup>+</sup> mode has a larger contribution from C–N displacements and more involvement from the peripheral rings. A similar picture is obtained for the other pair of vibrations at 1182 cm<sup>-1</sup> (**2**) and 1214 cm<sup>-1</sup> (**2**<sup>+</sup>). Thus the resonant enhancement in the monocation is favored by contributions from C–N and C–C stretches mainly associated with the outer phenyl rings. This indicates that the electronic absorption band being used to provide the resonant enhancement ( $\lambda_{\max}$  472 nm,  $n \rightarrow \pi^*$ ) involves a significant change in electron density on the

peripheral phenyl rings, which is entirely in agreement with our previous assignment of this band.<sup>12</sup>

Fig. 2 shows a plot of the Raman spectra of **2**<sup>+</sup> in the solid and solution state in the region below 1800 cm<sup>-1</sup>. There is obvious agreement between the spectra, and an excellent match in terms of the relative intensity of the various bands. The small frequency differences may be attributed to instrumental error. These similarities in spectral response between solution and solid state give further confidence in the applicability of these methods to the study of active devices.

While the use of an excitation wavelength of 514.5 nm results in resonance enhancement of the spectrum of the monocation **2**<sup>+</sup> due to the absorption band centered at 472 nm, there is much less resonance enhancement of the dication **2**<sup>2+</sup> at this excitation wavelength as the absorption band for this species centered at 492 nm is much less intense. For similar reasons, more intense Raman spectra are obtained from the dication **2**<sup>2+</sup> than the monocation **2**<sup>+</sup> with 632.7 nm excitation. The frequencies of the Raman active modes of the dication **2**<sup>2+</sup> are similar, but not identical, to those of the monocation **2**<sup>+</sup>. The observed **2**<sup>2+</sup> band at 1569 cm<sup>-1</sup> can be correlated with the cluster of calculated bands between 1569 and 1594 cm<sup>-1</sup> with the most intense of the predicted bands occurring at 1575 cm<sup>-1</sup> in the calculated vibrational profile (Fig. 7).

The enhanced bands at 1343 and 1395 cm<sup>-1</sup> in **2**<sup>2+</sup> are also of interest as these bands seem to be specific to the dication only. The observed band at 1343 cm<sup>-1</sup> is assigned to a cluster of calculated bands between 1303 and 1334 cm<sup>-1</sup> with the most intense predicted band being that at 1334 cm<sup>-1</sup>. These bands all involve combinations of C–C and C–N stretches. The displacements are similar in nature to those involved in the neutral band at 1294 cm<sup>-1</sup> and those in the monocation band at 1324 cm<sup>-1</sup>. The observed band at 1395 cm<sup>-1</sup> is assigned to a single calculated band at 1391 cm<sup>-1</sup>. This mode involves only the methyl groups and is similar in nature to those involved in the neutral band at 1371 cm<sup>-1</sup> and those in the monocation band at 1366 cm<sup>-1</sup>.

## Conclusions

The OTTLE cell combined with Raman spectroscopy provides an ideal way in which to generate and monitor the formation of radical species of charge transfer materials. In conjunction with DFT calculations it is possible to predict that the nature of the radical cations are best described in terms of a symmetrical, fully delocalized, radical structure.

Raman scattering from the two radical species is clearly different, allowing discrimination between the mono- and dications. The signal to noise ratios from the radicals in solution under resonance conditions are good, affording high levels of sensitivity. This suggests it may be possible to detect the radicals *in-situ* in a device at low concentrations. With a tuneable laser it should be possible to obtain resonance profiles for the monocation and dication, providing an effective way of probing structure.

## Acknowledgements

R. E. L. thanks the RSC and EPSRC for an analytical studentship, and Avecia Ltd. for a CASE award. M. A. J. P. was the recipient of an EPSRC/Avecia CASE for new academic appointees awarded to P. J. L. Other financial support to this project from EPSRC and Avecia (W. E. S.) is gratefully acknowledged.

## References

- 1 V. Bulvic, G. Gu, P. E. Burrows, S. R. Forrest and M. E. Thompson, *Nature*, 1996, **380**, 29.
- 2 N. Tamoto, C. Adachi and K. Nagai, *Chem. Mater.*, 1997, **9**, 1077.

- 3 E. Bellmann, S. E. Shaheen, S. Thayumanavan, S. Barlow, R. H. Grubbs, S. R. Marder, B. Kippelen and N. Peyghambarian, *Chem. Mater.*, 1998, **10**, 1668.
- 4 M. C. Harris and S. L. Buchwald, *J. Org. Chem.*, 2000, **65**, 5327.
- 5 U. Mitschke and P. Bäuerle, *J. Mater. Chem.*, 2000, **10**, 1471.
- 6 J. Cornil, N. E. Gruhn, D. A. dos Santos, M. Malagoli, P. A. Lee, S. Barlow, S. Thayumanavan, S. R. Marder, N. R. Armstrong and J. L. Bredas, *J. Phys. Chem. A*, 2001, **105**, 5206.
- 7 E. Bellmann, S. E. Shaheen, R. H. Grubbs, S. R. Marder, B. Kippelen and N. Peyghambarian, *Chem. Mater.*, 1999, **11**, 339.
- 8 M. V. d. Auwerer and F. C. D. Schryver, *J. Phys. Chem.*, 1993, **97**, 8808.
- 9 G. Pfister, *Phys. Rev. B*, 1977, **16**, 3676.
- 10 P. M. Borsenberger, W. Mey and A. Chowdry, *J. Appl. Phys.*, 1978, **49**, 273.
- 11 A. R. Kennedy, W. E. Smith, D. R. Tackley, W. I. F. David, K. Shankland, B. Brown and S. J. Teat, *J. Mater. Chem.*, 2002, **12**, 168.
- 12 P. J. Low, M. A. J. Paterson, H. Puschmann, A. E. Goeta, J. A. K. Howard, C. Lambert, J. C. Cherryman, D. R. Tackley, S. Leeming and B. Brown, *Chem. Eur. J.*, 2004, **10**, 83.
- 13 K. Sakanoue, M. Motoda, M. Sugimoto and S. Sakaki, *Nonlinear Optics*, 2000, **26**, 271.
- 14 I. Reva, L. Lapinski, N. Chattopadhyay and R. Fausto, *Phys. Chem. Chem. Phys.*, 2003, **5**, 3844.
- 15 M. Malagoli and J. L. Brédas, *Chem. Phys. Lett.*, 2000, **327**, 13.
- 16 K. Furuya, H. Torii, Y. Furukawa and M. Tasumi, *Theochem-J. Mol. Struct.*, 1998, **424**, 225.
- 17 K. Sakanoue, M. Motoda, M. Sugimoto and S. Sakaki, *J. Phys. Chem. A*, 1999, **103**, 5551.
- 18 C. Lambert and G. Nöll, *J. Am. Chem. Soc.*, 1999, **121**, 8434.
- 19 C. Lambert, G. Nöll and J. Schelter, *Nat. Mater.*, 2002, **1**, 69.
- 20 S. F. Nelson, *Chem. Eur. J.*, 2000, **6**, 581.
- 21 S. F. Nelson and H. Q. Tran, *J. Phys. Chem. A*, 1999, **103**, 8139.
- 22 S. F. Nelson, R. F. Ismagilov and D. R. Powell, *J. Am. Chem. Soc.*, 1997, **119**, 10213.
- 23 V. Guichard, A. Bourkba, M.-F. Lautie and O. Poizat, *Spectrochim. Acta A*, 1989, **45**, 187.
- 24 V. Guichard, O. Poizat and G. Buntinx, *J. Phys. Chem.*, 1989, **93**, 4436.
- 25 G. Buntinx and O. Poizat, *J. Phys. Chem.*, 1989, **91**, 2153.
- 26 R. E. Hester and K. P. J. Williams, *J. Chem., Soc. Faraday Trans. 2*, 1981, **77**, 541.
- 27 C. Kvarnström, A. Petr, P. Damlin, T. Lindfors, A. Ivaska and L. Dunsch, *J. Solid State Electrochem.*, 2002, **6**, 505.
- 28 A. E. Jones, C. A. Christensen, D. F. Perepichka, A. S. Batsanov, A. Beeby, P. J. Low, M. R. Bryce and A. W. Parker, *Chem. Eur. J.*, 2001, **7**, 973.
- 29 F. Hartl, T. L. Snoeck, D. J. Stufkens and A. B. P. Lever, *Inorg. Chem.*, 1995, **34**, 3887.
- 30 J.-S. Yu, C. Yang and H.-Q. Fang, *Anal. Chim. Acta*, 2000, **420**, 45.
- 31 L. Kavan, L. Dunsch and H. Kataura, *Chem. Phys. Lett.*, 2002, **361**, 79.
- 32 R. A. Fair, D. E. Ryan, P. K. Smith and P. R. Melarango, *Anal. Chem.*, 1986, **58**, 650.
- 33 P. A. Mosier-Boss, R. Newbery, S. Szpak, S. H. Lieberman and J. W. Rovang, *Anal. Chem.*, 1996, **68**, 3277.
- 34 P. Gau, *J. Electrochem. Soc.*, 1987, **134**, 654C.
- 35 R.-A. McNicholl, J. J. McGarvey, A. H. R. Al-Obaidi, S. E. J. Bell, P. M. Jayaweera and C. G. Coates, *J. Phys. Chem.*, 1995, **99**, 12268.
- 36 M. J. Plater and T. Jackson, *J. Chem. Soc., Perkin Trans. 1*, 2001, 2548.
- 37 C. M. Duff and G. A. Heath, *Inorg. Chem.*, 1991, **30**, 2528.
- 38 N. G. Connelly and W. E. Geiger, *Chem. Rev.*, 1996, **96**, 877.
- 39 M. J. Frisch, G. W. Trucks, H. B. Schlegel, G. E. Scuseria, M. A. Robb, J. R. Cheeseman, V. G. Zakrzewski, J. A. Montgomery, Jr., R. E. Stratmann, J. C. Burant, S. Dapprich, J. M. Millam, A. D. Daniels, K. N. Kudin, M. C. Strain, O. Farkas, J. Tomasi, V. Barone, M. Cossi, R. Cammi, B. Mennucci, C. Pomelli, C. Adamo, S. Clifford, J. Ochterski, G. A. Petersson, P. Y. Ayala, Q. Cui, K. Morokuma, D. K. Malick, A. D. Rabuck, K. Raghavachari, J. B. Foresman, J. Cioslowski, J. V. Ortiz, B. B. Stefanov, G. Liu, A. Liashenko, P. Piskorz, I. Komaromi, R. Gomperts, R. L. Martin, D. J. Fox, T. Keith, M. A. Al-Laham, C. Y. Peng, A. Nanayakkara, C. Gonzalez, M. Challacombe, P. M. W. Gill, B. G. Johnson, W. Chen, M. W. Wong, J. L. Andres, M. Head-Gordon, E. S. Replogle and J. A. Pople, *GAUSSIAN 98 (Revision A.9)*, Gaussian, Inc., Pittsburgh, PA, 1998.
- 40 A. D. Becke, *Phys. Rev. A*, 1988, **38**, 3098.
- 41 J. P. Perdew, K. Burke and Y. Wang, *Phys. Rev. B*, 1996, **54**, 16533.
- 42 R. Ditchfield, W. J. Hehre and J. A. Pople, *J. Chem. Phys.*, 1971, **54**, 724.
- 43 W. J. Hehre, R. Ditchfield and J. A. Pople, *J. Chem. Phys.*, 1972, **56**, 2257.
- 44 P. C. Hariharan and J. A. Pople, *Mol. Phys.*, 1974, **27**, 209.
- 45 M. S. Gordon, *Chem. Phys. Lett.*, 1980, **76**, 163.
- 46 P. C. Hariharan and J. A. Pople, *Theor. Chim. Acta.*, 1973, **28**, 213.
- 47 D. L. Rousseau, J. M. Friedman and P. F. Williams, *Top. Curr. Phys.*, 1979, **2**, 203.
- 48 R. E. Littleford, D. R. Tackley, J. C. Cherryman, G. Dent and W. E. Smith, *J. Mol. Struct.*, 2004, **692**, 81.